

Gapless excitations inside the fully gapped kagome superconductors AV_3Sb_5

Yuhao Gu,^{1,*} Yi Zhang,^{2,*} Xilin Feng,^{1,3} Kun Jiang,^{1,†} and Jiangping Hu^{1,2,‡}

¹Beijing National Laboratory for Condensed Matter Physics and Institute of Physics, Chinese Academy of Sciences, Beijing 100190, China

²Kavli Institute of Theoretical Sciences, University of Chinese Academy of Sciences, Beijing, 100190, China

³School of Physical Sciences, University of Chinese Academy of Sciences, Beijing 100190, China

(Dated: August 11, 2021)

The superconducting gap structures in the transition-metal-based kagome metal AV_3Sb_5 ($A=K,Rb,Cs$), the first family of quasi-two-dimensional kagome superconductors, remain elusive as there is strong experimental evidence for both nodal and nodalless gap structures. Here we show that the dichotomy can be resolved because of the coexistence of time-reversal symmetry breaking with a conventional fully gapped superconductivity. The symmetry protects the edge states which arise on the domains of the lattice symmetry breaking order to remain gapless in proximity to a conventional pairing. We demonstrate this result in a four-band tight-binding model using the $V d_{x^2-y^2}$ -like and the in-plane $Sb p_z$ -like Wannier functions that can faithfully capture the main feature of the materials near the Fermi level.

Because of their unique lattice structure, kagome materials have become an important platform for studying the interplay between electron correlation, topology and geometry frustration. Recently, the family of AV_3Sb_5 ($A=K,Rb,Cs$) materials has been found to be the first quasi-two-dimensional kagome superconductors (SC)[1–9]. These materials display many very intriguing phenomena. For example, an unconventional charge density wave (CDW) order has been found in the non-magnetic AV_3Sb_5 [1, 2, 10, 11], which is also concurrent with the anomalous Hall effect (AHE) [12]. Muon spin spectroscopy (μ SR) measurements [11, 13–15] have revealed solid evidence for time-reversal symmetry breaking (TRSB). In order to explain the TRSB, many theories have been proposed [16–20]. In particular, the chiral flux phase (CFP) [16], which carries unique nontrivial topological properties, can naturally explain the TRSB and AHE.

For the superconducting properties of AV_3Sb_5 , there are many controversial experimental results. On one hand, the superconductivity appears to be quite conventional. A Hebel-Slichter coherence peak appears just below the SC T_c from the spin-lattice relaxation measurement from the $^{121/123}Sb$ nuclear quadrupole resonance (NQR) [21]. The coherence peak is widely known as a hallmark for a conventional s -wave SC [22, 23], which is also consistent with the decreasing Knight shift after the SC transition [21]. The magnetic penetration depth measurements also suggest a full gapped superconducting state for CsV_3Sb_5 [15, 24]. There is also no magnetic resonance peak, which normally appears in superconductors with strong electron-electron correlation, such as cuprates and iron-based superconductors [25]. The weak electron-electron correlation in these materials is consistent with angle-resolved photoemission spectroscopy (ARPES) measurements [2, 26–32] and the first-principle calculations [33, 34]. In addition, the SC is very sensitive to magnetic impurities but without any resonance peaks to non-magnetic impurities [35]. The μ SR measurements also fail to detect any additional TRSB signals

below T_c , which indicates a time-reversal persevered SC order parameter [15]. On the other hand, the thermoelectric transport measurements show a finite residual thermal conductivity at $T \rightarrow 0$ in CsV_3Sb_5 , which indicates a nodal SC feature [5, 36]. Scanning tunneling microscopy (STM) observes the V-shape density of states (DOS), which is a typical feature for gapless SC [8, 9, 35]. As the existence of a gapless excitation normally indicates an unconventional superconductor, it is fundamentally important to find out a reconciliation of these experimental results.

In this paper, we suggest that because of the existence of TRSB, the gapless topological edge states are forbidden by symmetry from opening a gap by pairing in proximity to a conventional pairing. Thus, those gapless states on the domains of the CDW or hidden orders remain gapless in the superconducting states. Specifically, there are two key discrete symmetries in SCs to guarantee the presence of Cooper pairing, time-reversal T and inversion symmetry I [37–39]. Since the T maps a $|k, \uparrow\rangle$ state to $|-k, \downarrow\rangle$ state, the system at least contains time-reversal symmetry for the even-parity spin-singlet pairing formed by $(c_{k,\uparrow}c_{-k,\downarrow} - c_{k,\downarrow}c_{-k,\uparrow})$, as illustrated in Fig.1(a). In the same spirit, the odd-parity spin-triplet pairing needs inversion symmetry I owing to the fact that I maps a $|k, \uparrow\rangle$ state to $|-k, \uparrow\rangle$ state, as illustrated in Fig.1(b). These two symmetry conditions are known as the Anderson theorem [37–39]. For AV_3Sb_5 SC cases, due to TRSB, the normal states before the SC transition breaks the T symmetry. Therefore, the edge modes on CDW domain walls which break the T symmetry or other crystal grain boundaries cannot be gapped out by the SC, as illustrated in Fig.1(c). Hence, although the AV_3Sb_5 SC can be a conventional s -wave, it still contains gapless excitations. To demonstrate this physics, we construct a four band tight-binding (TB) model, which faithfully captures the band structures of AV_3Sb_5 near Fermi energy. Since the inversion symmetry is always a good symmetry for AV_3Sb_5 normal state from the recent second-harmonic generation measurement [14], the spin singlet pairing and spin triplet pairing should be separated. We will focus on the spin singlet in this work based on the decreasing Knight shift from NMR [21].

Since all AV_3Sb_5 materials have very similar band structures, we take CsV_3Sb_5 as an example. From the density func-

*These two authors contributed equally

[†]Electronic address: jiangkun@iphy.ac.cn

[‡]Electronic address: jphu@iphy.ac.cn

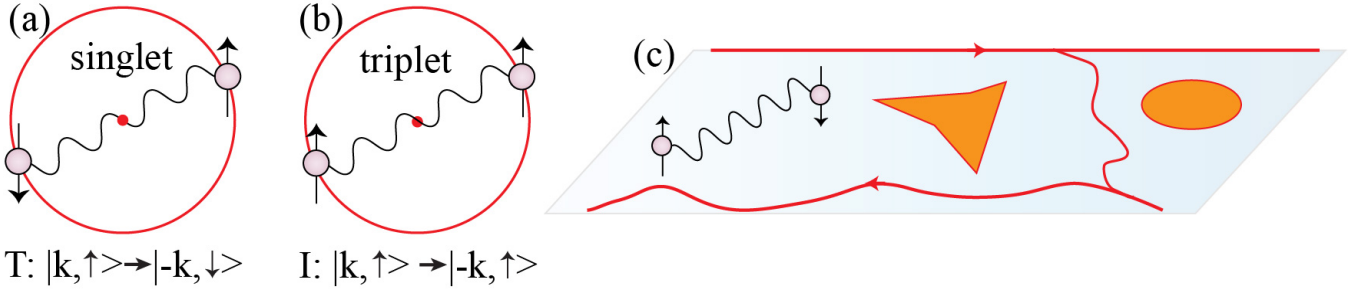


FIG. 1: (a) The time-reversal operator T maps a $|k, \uparrow\rangle$ state to $| -k, \downarrow\rangle$ state, which is the essential symmetry for spin singlet Cooper pairs. (b) The inversion operator I maps a $|k, \uparrow\rangle$ state to $| -k, \uparrow\rangle$ state, which is the essential symmetry for spin triplet Cooper pairs. (c) The edge states, CDW domain walls and other crystal grain boundaries etc. are not gapped out by the SC pairings.

tional theory (DFT) calculations and ARPES measurements [2, 26], there are multi-bands crossing the Fermi level, as shown in Fig.2(a). The crystal structure of CsV_3Sb_5 is shown in Fig.2(b-c). The DFT and ARPES results show that AV_3Sb_5 is a quasi-two-dimensional metal, whose electronic physics is dominated by electrons from the V-Sb plane [1, 2, 26]. In this V-Sb plane, three V atoms form a kagome lattice and an additional Sb atom forms a triangle lattice locating at the V hexagonal center. Above and below this V-Sb plane, out-of-plane Sb atoms form two honeycomb lattices respectively. Cs atoms form another triangle lattice above or below these Sb honeycomb planes.

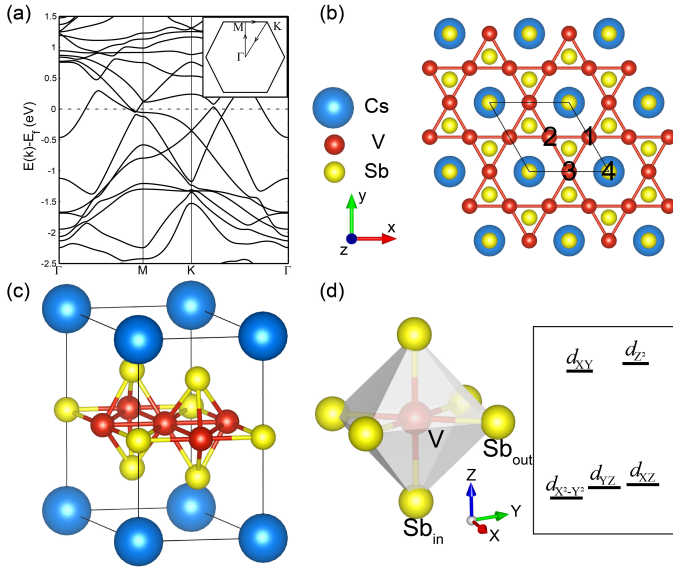


FIG. 2: (a) Band structure of CsV_3Sb_5 from DFT calculation with SOC. The inset shows the high symmetry \mathbf{k} -path we use. (b) Crystal structure of CsV_3Sb_5 from the top view. The Wannier centers of Wannier functions in the TB model are labeled as 1-4. (c) Crystal structure of CsV_3Sb_5 from the another angle view. (d) The illustration of the VSB_6 octahedra complex under the local coordinate $(X - Y - Z)$ and the schematic illustration for the crystal field splitting under this local coordinate. There are two types of Sb atoms: two Sb atoms are in the same plane with V atoms while the other four Sb atoms are out-of-plane.

We will show that a four-band TB model can faithfully cap-

ture the main physics behind AV_3Sb_5 based on Wannierization and symmetry analysis. To understand the band structure, we first focus on the local atomic structure of V atoms. There are three V atoms in the kagome lattice's unit cell (labeled as 1-3, as indicated in Fig.2(b)) and here we choose the local coordinate $(X - Y - Z)$ for each site, as shown in Fig.2(d). Let's take V-3 as an example to explain the definition of the local coordinate: as the global coordinate changes to the local coordinate, the axis $x/y/z$ turns to $Z/X/Y$ on V-3. By using C_3 symmetric operation, we can get the other two local coordinates on V-1 and V-2. In the local symmetric coordinate, the Z -axis always points to the in-plane Sb atom and the Y -axis is same as the z -axis in the global $x - y - z$ coordinate. The V atom can be considered as being coordinated in a distorted octahedron, whose point group symmetry is D_{2h} . The D_{2h} crystal field leads to no degeneracies of all the five d -orbitals (Fig.2(d)), consistent with our Wannierization result[40]. In the local coordinate, the energy of d_{XY}/d_{Z^2} orbital is higher than that of $d_{X^2-Y^2}/d_{XZ}/d_{YZ}$ orbital, similar to the familiar e_g-t_{2g} relationship in non-distorted octahedral crystal field.

From the DFT calculation and Wannierization, we find that the eigenstate of the von Hove(vH) point is mainly from the local $d_{X^2-Y^2}$ orbital discussed above. More importantly, the $d_{X^2-Y^2}$ orbital of this vH is dominated by the single V sublattice. This feature is the reason why a single orbital model on kagome lattice is a reasonable starting model for these materials [20, 41–43]. Namely, a minimal TB model based on the local $d_{X^2-Y^2}$ orbitals can capture the main physics of AV_3Sb_5 , especially the vH around the Fermi level. Besides the V d -orbital, there is one additional electron pocket around Γ point, which is attributed to the in-plane Sb's p_z orbital. Without the spin-orbital coupling (SOC), there is no overlap between the in-plane Sb p_z orbital and V $d_{X^2-Y^2}$ -orbital. Hence, the p_z band can be isolated from V $d_{X^2-Y^2}$ bands.

Based on the above observation, we apply the maximally localized Wannier functions (MLWFs) method to get the minimal model for CsV_3Sb_5 . Using the local V-centered $d_{X^2-Y^2}$ -like Wannier function, a three band model on kagome lattice is obtained as shown in Fig.3(b). The corresponding Wannier function is also plotted in Fig.3(a). By comparing with the DFT results in Fig.3(b), we find this three-band model well describes the main feature of vH points around the Fermi level and the Dirac cone at the K points. Additionally, using

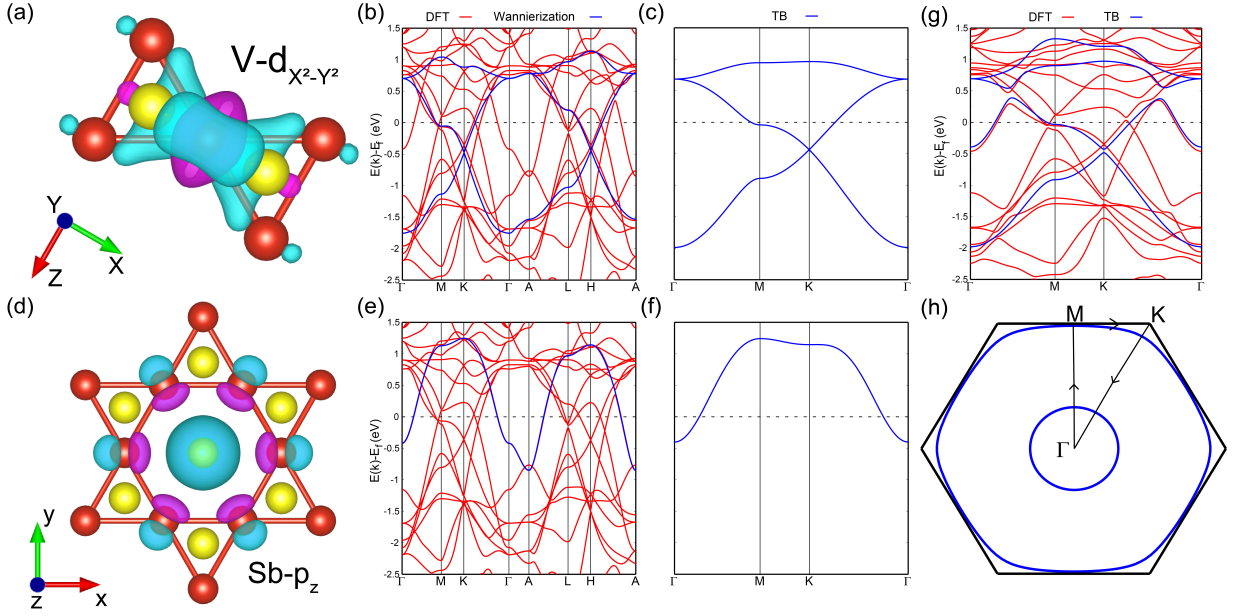


FIG. 3: (a) The $d_{x^2-y^2}$ -like Wannier function on V atom under the local $X - Y - Z$ coordinate. The other two $d_{x^2-y^2}$ -like Wannier functions are symmetric. (b) Band structures of CsV_3Sb_5 from DFT and Wannierization of three $d_{x^2-y^2}$ -like Wannier functions without SOC. (c) Band structure of the TB model with three $d_{x^2-y^2}$ -like Wannier functions. (d) The p_z -like Wannier function on in-plane Sb atom under the global $x - y - z$ coordinate. (e) Band structures of CsV_3Sb_5 from DFT and Wannierization of the p_z -like Wannier function without SOC. (f) Band structure of the TB model with the p_z -like Wannier function. (g) Band structure of the TB model with SOC. (h) The Fermi surface of the TB model.

the in-plane-Sb-centered p_z -like Wannier function, a single p_z band on triangle lattice is also obtained, as plotted in Fig.3(e). Its Wannier function is also shown in Fig.3(d). As shown in Fig.3(e), the Wannierized p_z band exactly agrees with the DFT calculation. Hence, the p_z band is isolated from other bands without SOC as discussed above. The SOC coupling terms can be further added in the minimal model using point group symmetry [40].

The effective TB model in the basis of three symmetric $d_{x^2-y^2}$ -like Wannier functions (labeled as 1-3) and one p_z -like Wannier function (labeled as 4) to describe the in-plane electronic physics, as shown in Fig.3(g). Including the SOC, the TB Hamiltonian can be written as

$$H_{TB} = H_V + H_{Sb} + H_{SOC}. \quad (1)$$

Details of this Hamiltonian with SOC can be found in the supplemental material [40].

Motivated by the chiral CDW found by magnetic-field dependent STM measurements [11] and its concurrence with AHE [12], several TRSB flux states have been proposed to explain the phenomena [16–20]. Among them, the lowest energy chiral flux phase (CFP) as shown in Fig.4(a) [16, 20] has gained support from recent μSR measurements [13, 14]. In the single orbital model, the CFP state has $C = 2$ Chern number [16]. The topological aspects of the CFP state in the minimal model remains the same as before. To confirm this, we carry out an open boundary calculation for the minimal model coupling with the CFP order. Note that we have ignored the Sb bands to avoid the complication. As shown in Fig.4(b), there are chiral edge states from non-zero Chern number inside the

bulk gap. It is important to point out that due to TRSB and inversion symmetry breaking at the boundary, the edge state spectrum has no relation between \mathbf{k} and $-\mathbf{k}$ anymore.

Now, we consider superconductivity in this system. The standard Bogoliubov-de Gennes (BdG) Hamiltonian can be written as

$$H_{BdG} = \begin{pmatrix} H_{TB}(k) - \mu & \hat{\Delta}(\mathbf{r}) \\ \hat{\Delta}^\dagger(\mathbf{r}) & -H_{TB}^T(-k) + \mu \end{pmatrix}, \quad (2)$$

in the basis $\Psi_k = (c_{k\uparrow}, c_{k\downarrow}, c_{-k\uparrow}^\dagger, c_{-k\downarrow}^\dagger)^T$, where μ is the chemical potential and $\hat{\Delta}(\mathbf{r})$ is the pairing function. We consider a standard s -wave function, $\hat{\Delta}(\mathbf{r}) = \Delta(\mathbf{r})i s_y$ with s_y the corresponding Pauli matrix in the spin space. Since our symmetry analysis and discussion does not depend on details of the microscopic model, we take the on-site s -wave pairing as an example, namely $\Delta(\mathbf{r}) = \Delta_{SC}$. As shown in Fig.4(c), the edge states remain gapless after the SC order is introduced. From Fig.4(b) and Fig.4(c), we can find that the energy difference δE between $E_{k,\uparrow}$ of the $|k, \uparrow\rangle$ state and $E_{-k,\downarrow}$ of the $| -k, \downarrow\rangle$ state is on the order of the TRSB gap Δ_{CFP} . Therefore, if the pairing gap Δ_{SC} is much smaller than δE , the edge states are always gapless. This result is still valid if we include the Sb band and the SOC term in the above calculation, as shown in Fig.4(d).

Experimentally, Δ_{CFP} is much larger than the Δ_{SC} in this family of materials. The μSR measurements show that the TRSB starts around $T \approx 70\text{K}$ for CsV_3Sb_5 with the CDW transition temperature $T \approx 90\text{K}$ [14]. The SC transition temperature is much smaller with $T_c \approx 2.5\text{K}$ [2]. Hence, re-

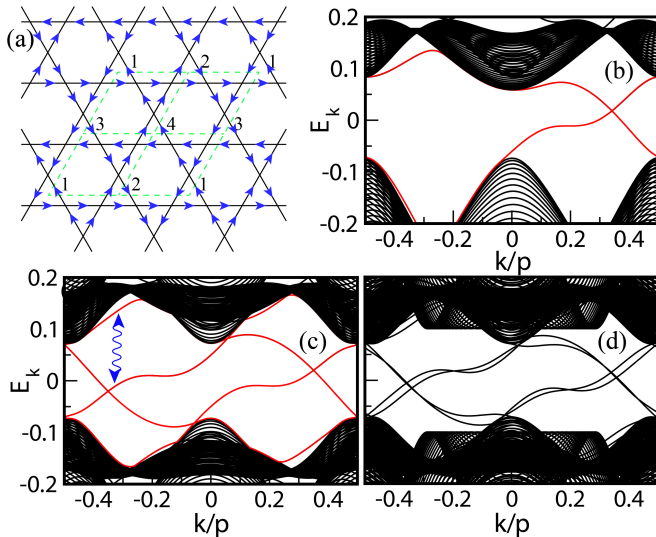


FIG. 4: (a) The hopping flux configuration for the chiral flux phase. (b) The edge states spectrum for the chiral flux phase without Sb bands. (c) The BdG spectrum for the pairing state without Sb bands. The energy difference δE between $E_{k,\uparrow}$ and $E_{-k,\downarrow}$ is on the order of Δ_{CFP} . (d) The BdG spectrum for the pairing state with Sb bands, where the SOC splits the in-gap bands. Here we take the CFP order parameter $\Delta_{CFP}=0.2$ eV and the onsite pairing for both V and Sb atoms to be $\Delta_{SC}=0.1$ eV and the chemical potential $\mu=-0.1$ eV. For the edge state calculation, we consider a system with translation invariance along \mathbf{a}_1 direction and open boundary condition along \mathbf{a}_2 direction with length of 100 lattice constant.

regardless of the microscopic pairing form, we expect that there are always gapless excitations in the edges, domain walls and other places of AV_3Sb_5 SC, where the TRSB order play a dominated role. This result can explain the residual thermal conductivity, where the gapless excitations contribute the thermal conductivity like the conventional electrons. It is clear that the above result can be extended to the spin-triplet pairing bulk state. In this case, the topological gapless states at the inversion symmetry broken structures can remain gapless.

In summary, we conclude that the AV_3Sb_5 ground state contains gapless excitations owing to its TRSB normal state even if the bulk superconductivity is fully gapped. To confirm this, a four-band TB model is constructed to capture electronic band structures of the materials, using the V-centered $d_{x^2-y^2}$ -like Wannier functions and the in-plane Sb-centered p_z -like Wannier function based on the technique of Wannierization and symmetry analysis. In this case, topological gapless excitations due to the TRSB remain gapless when a fully gapped SC order parameter is induced. Our proposal can be justified or falsified easily by measuring the states on edges or domain boundaries.

We thank Shiyan Li, Li Yu and Jiabin Yin for useful discussions. This work is supported by the Ministry of Science and Technology (Grant No. 2017YFA0303100), National Science Foundation of China (Grant No. NSFC-11888101), and the Strategic Priority Research Program of Chinese Academy of Sciences (Grant No. XDB28000000). K.J. acknowledges support from the start-up grant of IOP-CAS.

-
- [1] B. R. Ortiz et al., Phys. Rev. Mater. **3**, 094407 (2019).
[2] B. R. Ortiz et al., Phys. Rev. Lett. **125**, 247002 (2020).
[3] Brenden R. Ortiz, Paul M. Sarte, Eric M. Kenney, Michael J. Graf, Samuel M. L. Teicher, Ram Seshadri, and Stephen D. Wilson, Phys. Rev. Mater. **5**, 034801 (2021).
[4] Qiangwei Yin, Zhijun Tu, Chunsheng Gong, Yang Fu, Shaohua Yan, Hechang Lei, Chin. Phys. Lett. **38**, 037403 (2021).
[5] C. C. Zhao, L. S. Wang, W. Xia, Q. W. Yin, J. M. Ni, Y. Y. Huang, C. P. Tu, Z. C. Tao, Z. J. Tu, C. S. Gong, H. C. Lei, Y. F. Guo, X. F. Yang, S. Y. Li, arXiv:2102.08356.
[6] Feng Du, Shuaishuai Luo, Brenden R. Ortiz, Ye Chen, Weiyin Duan, Dongting Zhang, Xin Lu, Stephen D. Wilson, Yu Song, Huiqiu Yuan, arXiv:2102.10959.
[7] K. Y. Chen, N. N. Wang, Q. W. Yin, Z. J. Tu, C. S. Gong, J. P. Sun, H. C. Lei, Y. Uwatoko, J.-G. Cheng, arXiv:2102.09328.
[8] Zuwei Liang, Xingyuan Hou, Wanru Ma, Fan Zhang, Ping Wu, Zongyuan Zhang, Fanghang Yu, J. -J. Ying, Kun Jiang, Lei Shan, Zhenyu Wang, X. -H. Chen, arXiv:2103.04760.
[9] Hui Chen, Haitao Yang, Bin Hu, Zhen Zhao, Jie Yuan, Yuqing Xing, Guojian Qian, Zihao Huang, Geng Li, Yuhan Ye, Qiangwei Yin, Chunsheng Gong, Zhijun Tu, Hechang Lei, Shen Ma, Hua Zhang, Shunli Ni, Hengxin Tan, Chengmin Shen, Xiaoli Dong, Binghai Yan, Ziqiang Wang, Hong-Jun Gao, arXiv:2103.09188.
[10] Eric M. Kenney, Brenden R. Ortiz, Chennan Wang, Stephen D. Wilson, Michael J. Graf, arXiv:2012.04737.
[11] Y.-X. Jiang et al., arXiv:2012.15709.
[12] F. H. Yu, T. Wu, Z. Y. Wang, B. Lei, W. Z. Zhuo, J. J. Ying, X. H. Chen, arXiv:2102.10987.
[13] C. Mielke III, D. Das, J.-X. Yin, H. Liu, R. Gupta, C.N. Wang, Y.-X. Jiang, M. Medarde, X. Wu, H.C. Lei, J.J. Chang, P. Dai, Q. Si, H. Miao, R. Thomale, T. Neupert, Y. Shi, R. Khasanov, M.Z. Hasan, H. Luetkens, Z. Guguchia, arXiv:2106.13443.
[14] Li Yu, Chennan Wang, Yuhang Zhang, Mathias Sander, Shunli Ni, Zouyouwei Lu, Sheng Ma, Zhengguo Wang, Zhen Zhao, Hui Chen, Kun Jiang, Yan Zhang, Haitao Yang, Fang Zhou, Xiaoli Dong, Steven L. Johnson, Michael J. Graf, Jiangping Hu, Hong-Jun Gao, Zhongxian Zhao, arXiv:2107.10714.
[15] Ritu Gupta, Debarchan Das, Charles Hillis Mielke III, Zurab Guguchia, Toni Shiroka, Christopher Baines, Marek Bartkowiak, Hubertus Luetkens, Rustem Khasanov, Qiangwei Yin, Zhijun Tu, Chunsheng Gong, Hechang Lei, arXiv:2108.01574.
[16] Xilin Feng, Kun Jiang, Ziqiang Wang, Jiangping Hu, arXiv:2103.07097.
[17] M. Michael Denner and Ronny Thomale and Titus Neupert, arxiv:2103.14045.
[18] Yu-Ping Lin and Rahul M. Nandkishore, arXiv: 2104.02725.
[19] Takamori Park, Mengxing Ye, Leon Balents, arXiv: 2104.08425.
[20] Xilin Feng, Yi Zhang, Kun Jiang, Jiangping Hu, arXiv:2106.04395.
[21] Chao Mu, Qiangwei Yin, Zhijun Tu, Chunsheng Gong, Hechang Lei, Zheng Li, Jianlin Luo, Chin. Phys. Lett. **38**, 077402 (2021).
[22] L. C. Hebel and C. P. Slichter, Nuclear relaxation in superconducting aluminum, Phys. Rev. **107**, 901 (1957).
[23] L. C. Hebel and C. P. Slichter, Nuclear spin relaxation in normal and superconducting aluminum, Phys. Rev. **113**, 1504 (1959).

- [24] Weiyin Duan, Zhiyong Nie, Shuaishuai Luo, Fanghang Yu, Brenden R. Ortiz, Lichang Yin, Hang Su, Feng Du, An Wang, Ye Chen, Xin Lu, Jianjun Ying, Stephen D. Wilson, Xianhui Chen, Yu Song, Huiqiu Yuan, arXiv:2103.11796.
- [25] D. J. Scalapino, *Rev. Mod. Phys.* **84**, 1383 (2012).
- [26] Hailan Luo, Qiang Gao, Hongxiong Liu, Yuhao Gu, Dingsong Wu, Changjiang Yi, Junjie Jia, Shilong Wu, Xiangyu Luo, Yu Xu, Lin Zhao, Qingyan Wang, Hanqing Mao, Guodong Liu, Zhihai Zhu, Youguo Shi, Kun Jiang, Jiangping Hu, Zuyan Xu, X. J. Zhou, arXiv:2107.02688.
- [27] H. X. Li, T. T. Zhang, Y. Y. Pai, C. Marvinney, A. Said, T. Yilmaz, Q. Yin, C. Gong, Z. Tu, E. Vescovo, R. G. Moore, S. Murakami, H. C. Lei, H. N. Lee, B. Lawrie, and H. Miao, arXiv:2103.09769.
- [28] Zhengguo Wang, Sheng Ma, Yuhang Zhang, Haitao Yang, Zhen Zhao, Yi Ou, Yu Zhu, Shunli Ni, Zouyouwei Lu, Hui Chen, Kun Jiang, Li Yu, Yan Zhang, Xiaoli Dong, Jiangping Hu, HongJun Gao, and Zhongxian Zhao, arXiv:2104.05556.
- [29] Kosuke Nakayama, Yongkai Li, Min Liu, Zhiwei Wang, Takashi Takahashi, Yugui Yao, and Takafumi Sato, arXiv:2104.08042.
- [30] Yang Luo, Shuting Peng, Samuel M. L. Teicher, Linwei Huai, Yong Hu, Brenden R. Ortiz, Zhiyuan Wei, Jianchang Shen, Zhipeng Ou, Bingqian Wang, Yu Miao, Mingyao Guo, M. Shi, Stephen D. Wilson, and J. F. He, arXiv:2106.01248.
- [31] Zhonghao Liu, Ningning Zhao, Qiangwei Yin, Chunsheng Gong, Zhijun Tu, Man Li, Wenhua Song, Zhengtai Liu, Dawei Shen, Yaobo Huang, Kai Liu, Hechang Lei, and Shancai Wang, arXiv:2104.01125.
- [32] Yong Hu, Samuel M. L. Teicher, Brenden R. Ortiz, Yang Luo, Shuting Peng, Linwei Huai, J. Z. Ma, N. C. Plumb, Stephen D. Wilson, J. F. He, and M. Shi, arXiv:2104.12725.
- [33] Jian-Feng Zhang, Kai Liu, Zhong-Yi Lu, arXiv:2106.11477.
- [34] Jianzhou Zhao, Weikang Wu, Yilin Wang, Shengyuan A. Yang, *Phys. Rev. B* **103**, 241117 (2021).
- [35] Han-Shu Xu, Ya-Jun Yan, Ruotong Yin, Wei Xia, Shijie Fang, Ziyuan Chen, Yuanji Li, Wenqi Yang, Yanfeng Guo, Dong-Lai Feng, arXiv:2104.08810.
- [36] Xianxin Wu et al., arXiv:2104.05671.
- [37] P.W. Anderson, *J. Phys. Chem. Solids* **11**, 26 (1959).
- [38] P.W. Anderson, *Phys. Rev. B* **30**, 4000 (1984).
- [39] M. Sigrist, *AIP Conf. Proc.* **1162**, 55 (2009).
- [40] See Supplemental Material for more detailed discussions.
- [41] Shun-Li Yu and Jian-Xin Li, *Phys. Rev. B* **85**, 144402 (2012).
- [42] Wan-Sheng Wang, Zheng-Zhao Li, Yuan-Yuan Xiang, and Qiang-Hua Wang, *Phys. Rev. B* **87**, 115135 (2013).
- [43] Maximilian L. Kiesel, Christian Platt, and Ronny Thomale, *Phys. Rev. Lett.* **110**, 126405 (2013).

Supplemental Material for "Gapless excitations inside the fully gapped kagome superconductors AV_3Sb_5 "

I. COMPUTATIONAL DETAILS

Our density functional theory calculations employ the Vienna ab initio simulation package (VASP) code[1] with the projector augmented wave (PAW) method[2]. The Perdew-Burke-Ernzerhof (PBE)[3] exchange-correlation functional is used in our calculations. The kinetic energy cutoff is set to be 600 eV for the expanding the wave functions into a plane-wave basis in VASP calculations while the energy convergence criterion is 10^{-6} eV. The experimental crystal structures of AV_3Sb_5 (A=K,Rb,Cs) are adopted[4]. The Γ -centered \mathbf{k} -mesh is $12 \times 12 \times 7$.

We employ Wannier90[5, 6] to calculate maximally localized Wannier functions. We get our TB model's parameters by fitting the band structure from the Wannierization.

II. WANNIERIZATION WITH V'S d -ORBITALS AND Sb'S p -ORBITALS

Our Wannierization with V's d -orbitals and Sb's p -orbitals can perfectly reproduce band structure from DFT, as shown in FIG.S1. In our local coordinate, there are five different parts which cross the Fermi level, as labeled in FIG.S2. The a1/a2 part, forming a vH singularity at M point and a Dirac cone at K point, is mainly attributed to $V-d_{YZ}/X^2-Y^2$ orbital, as shown in FIG.S2(a). The a1/a2 part crosses the Fermi level along $\Gamma - M$ line and $K - \Gamma$, respectively. The b1 band (FIG.S2(b)), mainly composed of $V-d_{XY}$ orbital and also hybridizing with Sb_{out-p_y} orbital, crosses the Fermi level along the $K - \Gamma$ line. Moreover, the c1 band in FIG.S2(c) clearly indicates that Sb_{in-p_z} orbital can be isolated around the Fermi energy and forms an electron pocket around the Γ point. In FIG.S2(d), the d1 band, chiefly contributed by Sb_{out-p_y} orbital, crosses the Fermi level along $\Gamma - M$ line. It is worthy noting that our $\Gamma - M$ line is same as the direction of the global y -axis (FIG.S4(a)), thus Sb's p_y component will change to a symmetric linear combination of Sb's p_x and p_y orbitals as rotate M to M' or M'' .

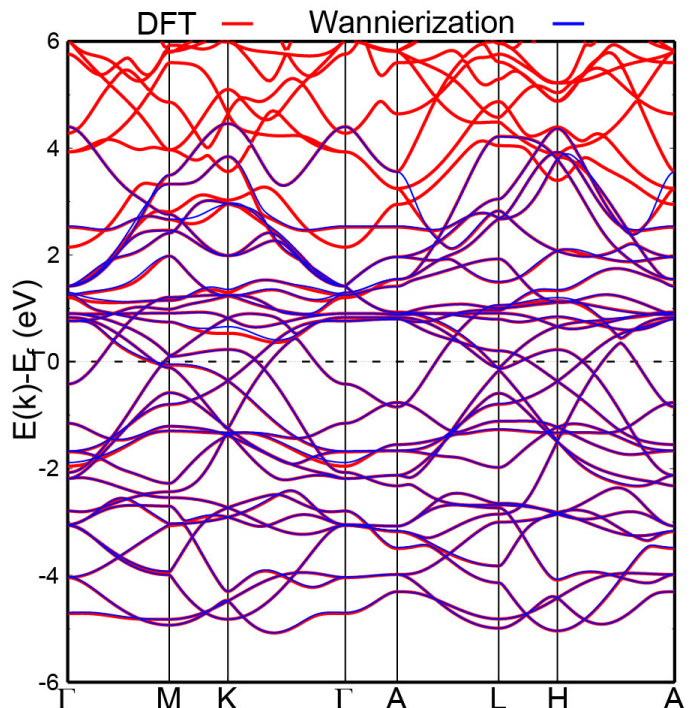


FIG. S1: (color online) Comparison between band structures from DFT and Wannierization with V's d -orbitals and Sb's p -orbitals in CsV_3Sb_5 .

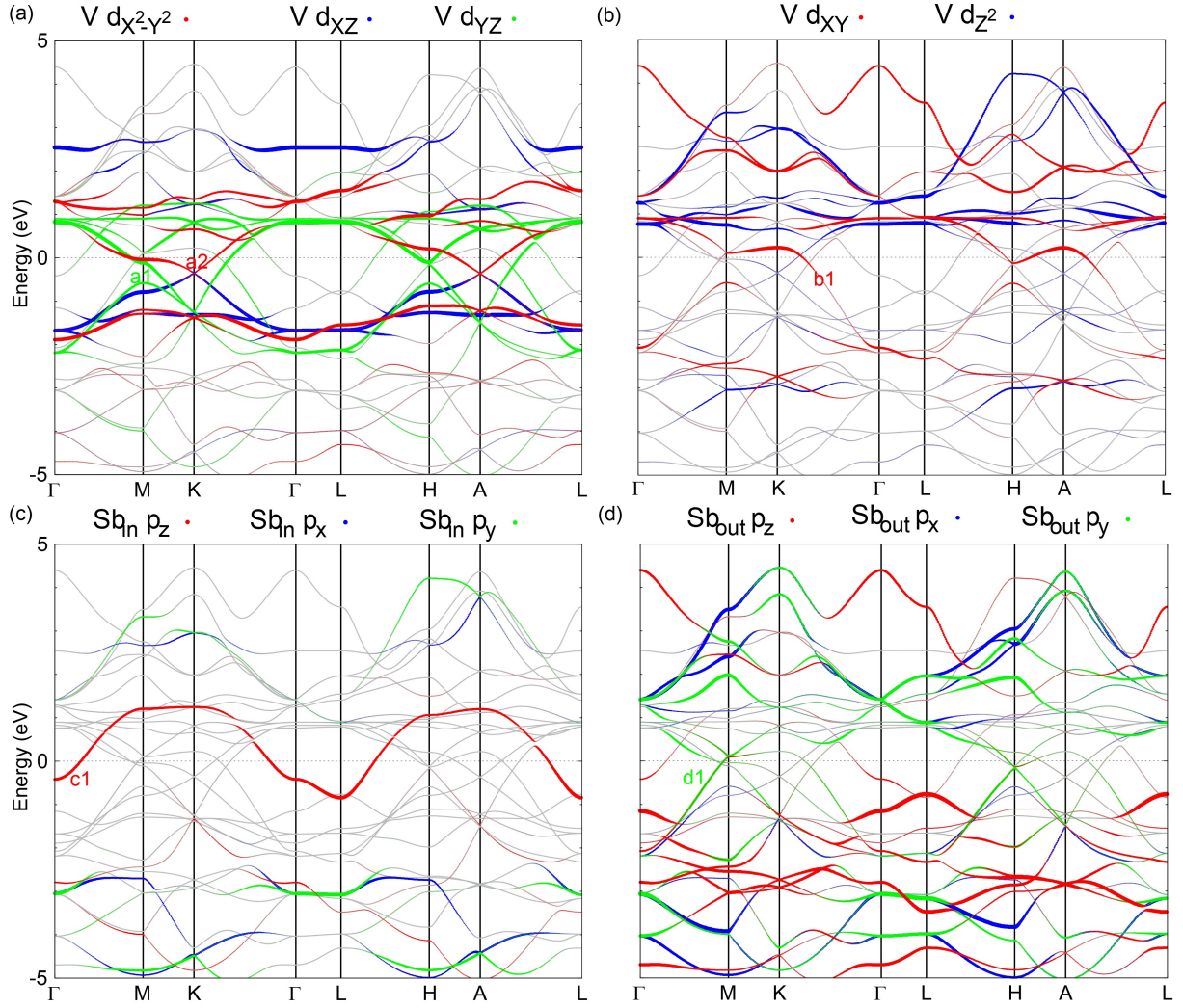


FIG. S2: (color online) CsV_3Sb_5 's projected band structures without spin-orbit coupling (SOC) from Wannierization of V's d -orbitals and Sb's p -orbitals. The bands crossing the Fermi level are labeled as a1, a2, b1, c1 and d1, which are mainly composed by $V-d_{yz}$ orbital, $V-d_{x^2-y^2}$ orbital, $V-d_{xy}$ orbital, $Sb_{in}-p_z$ orbital and $Sb_{out}-p_y$ orbital, respectively.

III. EFFECTIVE 4-BAND TB MODEL

We construct the effective TB model in the basis of three symmetric $d_{x^2-y^2}$ -like Wannier functions (labeled as 1-3) and one p_z -like Wannier function (labeled as 4) to describe the in-plane electronic physics:

$$\Psi^\dagger = (\Phi_{d_{x^2-y^2},V1}^\dagger, \Phi_{d_{x^2-y^2},V2}^\dagger, \Phi_{d_{x^2-y^2},V3}^\dagger, \Phi_{p_z,Sb_m}^\dagger) \quad (S1)$$

$$\begin{aligned} H_{11} &= \varepsilon_V + 2t_{TNN}^1 \cos(-k_x/2 + \sqrt{3}k_y/2) + 2t_{TNN}^2 (\cos(k_x) + \cos(k_x/2 + \sqrt{3}k_y/2)), \\ H_{22} &= \varepsilon_V + 2t_{TNN}^1 \cos(k_x/2 + \sqrt{3}k_y/2) + 2t_{TNN}^2 (\cos(k_x) + \cos(-k_x/2 + \sqrt{3}k_y/2)), \\ H_{33} &= \varepsilon_V + 2t_{TNN}^1 \cos(k_x) + 2t_{TNN}^2 (\cos(k_x/2 + \sqrt{3}k_y/2) + \cos(-k_x/2 + \sqrt{3}k_y/2)), \\ H_{44} &= \varepsilon_{Sb} + 2t_{NN}^{Sb} (\cos(k_x) + \cos(-k_x/2 + \sqrt{3}k_y/2) + \cos(k_x/2 + \sqrt{3}k_y/2)) \\ &\quad + 2t_{SNN}^{Sb} (\cos(3k_x/2 - \sqrt{3}k_y/2) + \cos(3k_x/2 + \sqrt{3}k_y/2) + \cos(\sqrt{3}k_y)) \\ H_{12} &= 2t_{NN} \cos(k_x/2) + 2t_{SNN} \cos(\sqrt{3}k_y/2), \\ H_{13} &= 2t_{NN} \cos(k_x/4 + \sqrt{3}k_y/4) + 2t_{SNN} \cos(3k_x/4 - \sqrt{3}k_y/4), \\ H_{23} &= 2t_{NN} \cos(-k_x/4 + \sqrt{3}k_y/4) + 2t_{SNN} \cos(3k_x/4 + \sqrt{3}k_y/4), \\ H_{14} &= H_{24} = H_{34} = 0. \end{aligned} \quad (S2)$$

Our hopping parameters are truncated between third nearest neighbours (TNN) on V sites and second nearest neighbours on Sb sites, whose definitions are shown in FIG.S4(a). We get hopping parameters and on-site energies by fitting the band structure of Wannierization as in Ref.[7] (TABLE.S1).

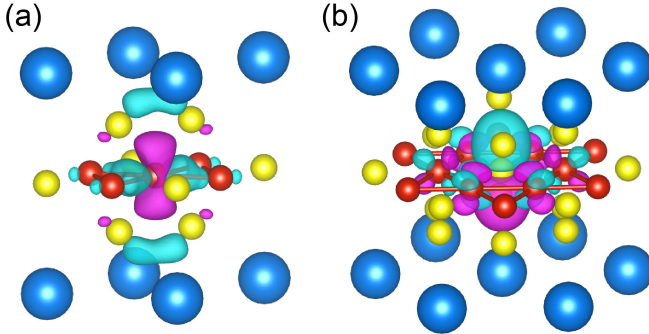


FIG. S3: (color online) (a) V-centered $d_{x^2-y^2}$ -like Wannier function and (b) Sb-centered p_z -like Wannier function in our 4-band TB model from another angle of view.

We plot these Wannier functions from another angle of view in FIG.S3. The TB model can be written as a 4×4 Hermitian matrix (H_{TB}):

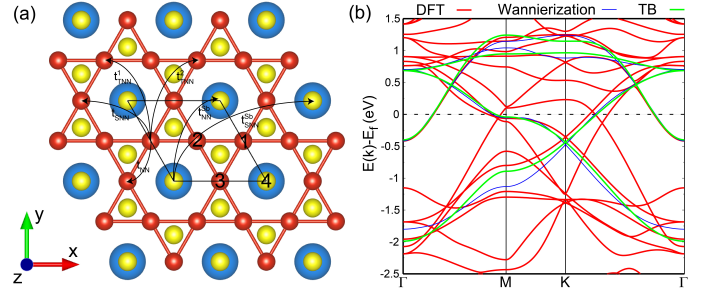


FIG. S4: (color online) (a) Definitions of hopping parameters in our TB model. (b) band structures of CsV_3Sb_5 from DFT, Wannierization and TB model without SOC.

TABLE S1: The parameters in our 4-band TB model. The unit is eV here.

ε_V	-0.0480
t_{NN}	-0.453
t_{SNN}	0.00713
t_{TNN}^1	-0.0377
t_{TNN}^2	-0.0205
ε_{Sb}	0.831
t_{NN}^{Sb}	-0.172
t_{SNN}^{Sb}	-0.0335

IV. SPIN-ORBITAL COUPLING

From main text, we can see that the couplings between p_z and d bands are mostly from the spin-orbital coupling (SOC). For example, a non-negligible gap between V's band and Sb's band along $\Gamma - M$ line owing to SOC, as shown in FIG.S5(b). Based on point group symmetry, one can generate all possible SOC coupling terms in our minimal model. The procedure is following. Taking V-3's orbital and its nearest neighbouring in-plane Sb's orbital as an example, the general form of SOC is

$$H_{SOC}^{V_3-Sb} = ac_{V_3\uparrow}^+ c_{Sb\uparrow} + bc_{V_3\uparrow}^+ c_{Sb\downarrow} + cc_{V_3\downarrow}^+ c_{Sb\uparrow} + dc_{V_3\downarrow}^+ c_{Sb\downarrow} + h.c. \quad (S3)$$

This term can be simplified with time-reversal symmetry, rotation symmetry C_{2x} and mirror symmetry M_{xy} , which are shown in FIG.S5(a). With time-reversal symmetry, we can get $a = d^*, b = -c^*$, so the SOC term can be expressed as:

$$H_{SOC}^{V_3-Sb} = ac_{V_3\uparrow}^+ c_{Sb\uparrow} + bc_{V_3\uparrow}^+ c_{Sb\downarrow} - b^* c_{V_3\downarrow}^+ c_{Sb\uparrow} + a^* c_{V_3\downarrow}^+ c_{Sb\downarrow} + h.c.. \quad (S4)$$

Then we can simplify the SOC term further by considering symmetry operators C_{2x} and M_{xy} , as shown in FIG.S5(a). The rotation symmetry C_{2x} leads $a = -a^* = i\lambda, b = b^*$ (λ and b are real numbers). Namely, the SOC term can be written as:

$$H_{SOC}^{V_3-Sb} = i\lambda(c_{V_3\uparrow}^+ c_{Sb\uparrow} - c_{V_3\downarrow}^+ c_{Sb\downarrow}) + b(c_{V_3\uparrow}^+ c_{Sb\downarrow} - c_{V_3\downarrow}^+ c_{Sb\uparrow}) + h.c.. \quad (S5)$$

With considering the mirror symmetry M_{xy} , we can have $\lambda = 0$. As a result, the SOC term between V3's orbital and Sb's orbital now is simplified as:

$$H_{SOC}^{V_3-Sb} = b(c_{V_3\uparrow}^+ c_{Sb\downarrow} - c_{V_3\downarrow}^+ c_{Sb\uparrow}) + h.c.. \quad (S6)$$

The rotation symmetry C_{2z} leads the SOC term changes sign when switching two in-plane Sb atoms, so the SOC term on lattice becomes:

$$H_{SOC}^{V_3-Sb} = \sum_{ij} b(c_{V_3i\uparrow}^+ c_{Sbj\uparrow+\frac{a_1}{2}\downarrow} - c_{V_3ij\downarrow}^+ c_{Sbj\uparrow+\frac{a_1}{2}\uparrow}) - b(c_{V_3ij\uparrow}^+ c_{Sbj\uparrow-\frac{a_1}{2}\downarrow} - c_{V_3ij\downarrow}^+ c_{Sbj\uparrow-\frac{a_1}{2}\uparrow}) + h.c.. \quad (S7)$$

With Fourier transformation, it becomes:

$$H_{SOC}^{V_3-Sb}(\vec{k}) = \sum_{\vec{k}} 2ib\sin(\frac{k_x}{2})(c_{V_3\vec{k}\uparrow}^+ c_{Sb\vec{k}\downarrow} - c_{V_3\vec{k}\downarrow}^+ c_{Sb\vec{k}\uparrow}) + h.c.. \quad (S8)$$

By rotation symmetry, we can derive the remaining SOC term between V1/V2's orbital and Sb's orbital:

$$H_{SOC}^{V_1-Sb} = \sum_{\vec{k}} 2ib\sin(\frac{-k_x + \sqrt{3}k_y}{4})((-\frac{1}{2} + i\frac{\sqrt{3}}{2})c_{V_1\vec{k}\uparrow}^+ c_{Sb\vec{k}\downarrow} + (\frac{1}{2} + i\frac{\sqrt{3}}{2})c_{V_1\vec{k}\downarrow}^+ c_{Sb\vec{k}\uparrow}) + h.c., \quad (S9)$$

$$H_{SOC}^{V_2-Sb} = \sum_{\vec{k}} 2ib\sin(\frac{k_x + \sqrt{3}k_y}{4})((\frac{1}{2} + i\frac{\sqrt{3}}{2})c_{V_2\vec{k}\uparrow}^+ c_{Sb\vec{k}\downarrow} - (\frac{1}{2} - i\frac{\sqrt{3}}{2})c_{V_2\vec{k}\downarrow}^+ c_{Sb\vec{k}\uparrow}) + h.c.. \quad (S10)$$

With considering SOC, the full Hamiltonian is an 8×8 Hermitian matrix owing to the spin degree of freedom:

$$H = \begin{pmatrix} H_{TB} & H_{SOC} \\ H_{SOC}^\dagger & H_{TB} \end{pmatrix} \quad (S11)$$

The matrix elements for SOC is in off-diagonal block (H_{SOC}):

$$\begin{aligned} H_{18} &= H_{4,5} = b\sin(\frac{-k_x + \sqrt{3}k_y}{4})(-\sqrt{3} - i), \\ H_{28} &= H_{4,6} = b\sin(\frac{k_x + \sqrt{3}k_y}{4})(-\sqrt{3} + i), \\ H_{38} &= H_{4,7} = b\sin(\frac{k_x}{2})i, \\ H_{15} &= H_{16} = H_{17} = H_{25} = H_{26} = H_{27} \\ &= H_{35} = H_{36} = H_{37} = H_{48} = 0. \end{aligned} \quad (S12)$$

Now there is only one parameter b . Here we estimate $b = 0.1$ eV, and the corresponding band structure is plotted in FIG.S5(b). Gaps open because bands become the same double group representation.

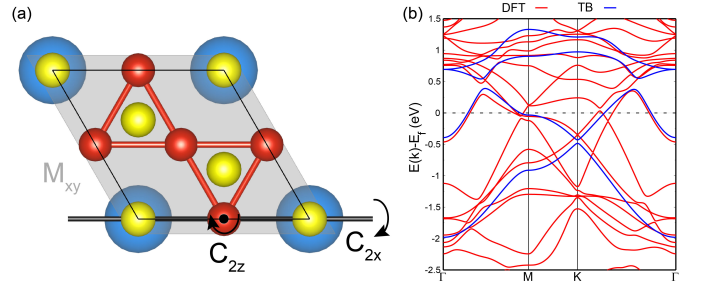


FIG. S5: (color online) (a) Schematic illustration for mirror symmetry M_{xy} and rotation symmetry C_{2x}/C_{2z} in CsV_3Sb_5 . (b) Band structures of CsV_3Sb_5 from DFT and the TB model with SOC.

V. AN ALTERNATIVE 7-BAND TB MODEL

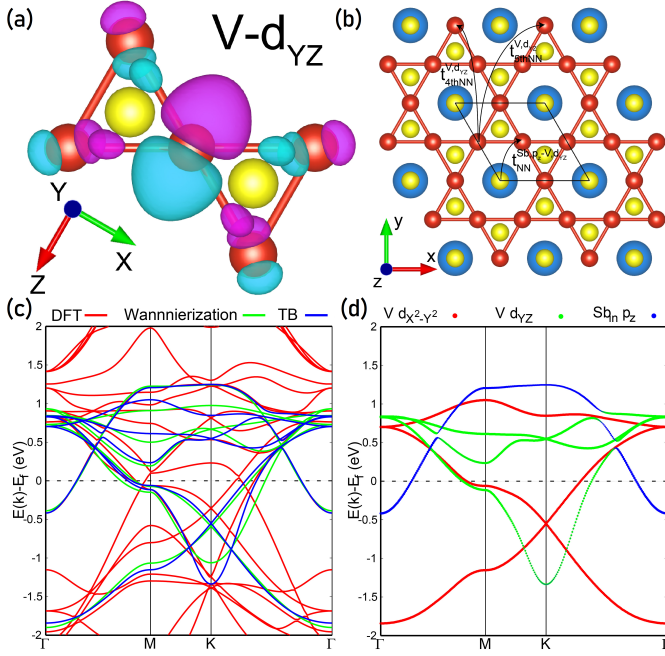


FIG. S6: (color online) (a) The d_{YZ} -like Wannier function on V atom under the local X-Y-Z coordinate. (b) Definitions of new hopping parameters in our 7-band TB model. (c) Band structures from DFT, Wannierization and 7-band TB model. (d) Fat band analysis from Wannierization and the sizes of the dots represent the weight of the projection.

$$\Psi^\dagger = (\Phi_{d_{x^2-y^2}, V1}^\dagger, \Phi_{d_{x^2-y^2}, V2}^\dagger, \Phi_{d_{x^2-y^2}, V3}^\dagger, \Phi_{p_z, Sb_{in}}^\dagger, \Phi_{d_{YZ}, V1}^\dagger, \Phi_{d_{YZ}, V2}^\dagger, \Phi_{d_{YZ}, V3}^\dagger). \quad (S13)$$

The V-centered d_{YZ} -like Wannier function is plotted in FIG.S6(a). So we similarly get a faithful Wannierization result with 7 initial projectors, as shown in FIG.S6(c). Owing to the symmetry, the V-centered $d_{x^2-y^2}$ -like Wannier function does not hybridize with the Sb_{in} -centered p_z -like Wannier function, while the V-centered d_{YZ} -like Wannier function does, as shown in our fat band analysis (FIG.S6(d)).

The 7×7 TB model has the following structure:

$$H_{TB}^{7band} = \begin{pmatrix} H^{d_{x^2-y^2}} & 0 & 0 & 0 & 0 \\ 0 & 0 & 0 & 0 & 0 \\ 0 & 0 & 0 & 0 & 0 \\ 0 & 0 & 0 & H^{p_z} & V^{p_z-d_{YZ}} \\ 0 & 0 & 0 & V^\dagger p_z-d_{YZ} & H^{d_{YZ}} \\ 0 & 0 & 0 & 0 & 0 \end{pmatrix} \quad (S14)$$

As mentioned before (FIG.S2), there are two vH points near the Fermi level, which indicates a two-orbital model[8, 9]. In our local coordinate, the lower vH point is mainly composed by V's d_{YZ} orbital. Therefore, we can alternatively construct a 7-band TB model which can describe both in the basis:

The analytical terms of $H^{d_{x^2-y^2}}$ and H^{p_z} in 7-band TB model are same as those in the 4-band TB model. To get a decent fitting result, we need to consider longer hopping between V's 4/5th nearest neighbouring sites, as shown in FIG.S6(b). The adding terms in H_{TB}^{7band} can be written as:

$$\begin{aligned}
H_{55} &= \varepsilon_V^{dyz} + 2t_{TNN}^{V,dyz,1} \cos(-k_x/2 + \sqrt{3}k_y/2) + 2t_{TNN}^{V,dyz,2} (\cos(k_x) + \cos(k_x/2 + \sqrt{3}k_y/2)), \\
H_{66} &= \varepsilon_V^{dyz} + 2t_{TNN}^{V,dyz,1} \cos(k_x/2 + \sqrt{3}k_y/2) + 2t_{TNN}^{V,dyz,2} (\cos(k_x) + \cos(-k_x/2 + \sqrt{3}k_y/2)), \\
H_{77} &= \varepsilon_V^{dyz} + 2t_{TNN}^{V,dyz,1} \cos(k_x) + 2t_{TNN}^{V,dyz,2} (\cos(k_x/2 + \sqrt{3}k_y/2) + \cos(-k_x/2 + \sqrt{3}k_y/2)), \\
H_{56} &= 2t_{NN}^{V,dyz} \cos(k_x/2) + 2t_{SNN}^{V,dyz} \cos(\sqrt{3}k_y/2) \\
&\quad + 2t_{4thNN}^{V,dyz} (\cos(k_x + \sqrt{3}k_y/2) + \cos(k_x - \sqrt{3}k_y/2)) + 2t_{5thNN}^{V,dyz} \cos(3k_x/2), \\
H_{57} &= 2t_{NN}^{V,dyz} \cos(k_x/4 + \sqrt{3}k_y/4) + 2t_{SNN}^{V,dyz} \cos(3k_x/4 - \sqrt{3}k_y/4) \\
&\quad + 2t_{4thNN}^{V,dyz} (\cos(5k_x/4 + \sqrt{3}k_y/4) + \cos(-k_x/4 + 3\sqrt{3}k_y/4)) + 2t_{5thNN}^{V,dyz} \cos(3k_x/4 + 3\sqrt{3}k_y/4), \\
H_{23} &= 2t_{NN}^{V,dyz} \cos(-k_x/4 + \sqrt{3}k_y/4) + 2t_{SNN}^{V,dyz} \cos(3k_x/4 + \sqrt{3}k_y/4) \\
&\quad + 2t_{4thNN}^{V,dyz} (\cos(k_x/4 + 3\sqrt{3}k_y/4) + \cos(5k_x/4 - \sqrt{3}k_y/4)) + 2t_{5thNN}^{V,dyz} \cos(-3k_x/4 + 3\sqrt{3}k_y/4), \\
H_{45} &= -2it_{NN}^{Sb,p_z-V,dyz} \sin(-k_x/4 + \sqrt{3}k_y/4), \\
H_{46} &= 2it_{NN}^{Sb,p_z-V,dyz} \sin(k_x/4 + \sqrt{3}k_y/4), \\
H_{47} &= -2it_{NN}^{Sb,p_z-V,dyz} \sin(k_x/2).
\end{aligned} \tag{S15}$$

This 7-band TB model can faithfully fit the DFT-calculated band structure, as shown in FIF.S6(c). This result also reveals the two orbital nature of the two vH singularities around the Fermi level: one vH point is composed by local $d_{x^2-y^2}$ -like Wannier function, whose NN hopping is dominating; another vH is composed by local d_{YZ} -like Wannier function, whose TNN hopping is the biggest.

It is worthy noting that the d_{YZ} -composed vH will be the nearest vH to the Fermi level in KV_3Sb_5/RbV_3Sb_5 , as shown in FIG.S7. This might be a significant difference between CsV_3Sb_5 and KV_3Sb_5/RbV_3Sb_5 .

TABLE S2: The parameters in our 7-band TB model. The unit is eV here.

$\varepsilon_V^{d_{x^2-y^2}}$	-0.0946
$t_{NN}^{V,d_{x^2-y^2}}$	-0.4661
$t_{SNN}^{V,d_{x^2-y^2}}$	0.0278
$t_{TNN}^{V,d_{x^2-y^2},1}$	-0.008
$t_{TNN}^{V,d_{x^2-y^2},2}$	-0.0091
$\varepsilon_V^{p_z}$	0.8215
t_{NN}^{Sb,p_z}	-0.1813
t_{SNN}^{Sb,p_z}	-0.0204
$\varepsilon_V^{d_{YZ}}$	0.3619
$t_{NN}^{V,d_{YZ}}$	0.1112
$t_{SNN}^{V,d_{YZ}}$	-0.1168
$t_{TNN}^{V,d_{YZ},1}$	0.0077
$t_{TNN}^{V,d_{YZ},2}$	0.1315
$t_{4thNN}^{V,d_{YZ}}$	0.0356
$t_{5thNN}^{V,d_{YZ}}$	-0.0802
$t_{NN}^{Sb,p_z-V,dyz}$	-0.0071

[1] G. Kresse and J. Furthmüller, Phys. Rev. B **54**, 11169 (1996).
[2] G. Kresse and D. Joubert, Phys. Rev. B **59**, 1758 (1999).

[3] J. P. Perdew, K. Burke, and M. Ernzerhof, Phys. Rev. Lett. **77**, 3865 (1996).

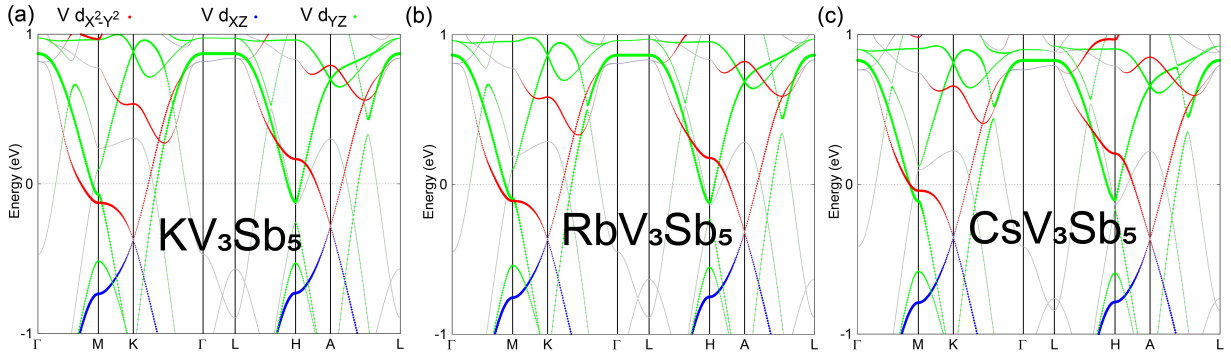


FIG. S7: (color online) Projected band structures without SOC from Wannierization of V's d -orbitals and Sb's p -orbitals for (a)KV₃Sb₅, (b)RbV₃Sb₅ and (c)CsV₃Sb₅ .

- [4] B. R. Ortiz, L. C. Gomes, J. R. Morey, M. Winiarski, M. Bordelon, J. S. Mangum, I. W. Oswald, J. A. Rodriguez-Rivera, J. R. Neilson, S. D. Wilson, *et al.*, *Phys. Rev. Mater.* **3**, 094407 (2019).
- [5] A. A. Mostofi, J. R. Yates, Y.-S. Lee, I. Souza, D. Vanderbilt, and N. Marzari, *Comput. Phys. Commun.* **178**, 685 (2008).
- [6] N. Marzari, A. A. Mostofi, J. R. Yates, I. Souza, and D. Vanderbilt, *Rev. Mod. Phys.* , 1419 (2012).
- [7] Y. Gu, X. Wu, K. Jiang, and J. Hu, *Chin. Phys. Lett.* **38**, 017501 (2021).
- [8] M. Kang, S. Fang, J.-K. Kim, B. R. Ortiz, J. Yoo, B.-G. Park, S. D. Wilson, J.-H. Park, and R. Comin, arXiv preprint arXiv:2105.01689 (2021).
- [9] X. Wu, T. Schwemmer, T. Muller, A. Consiglio, G. Sangiovanni, D. D. Sante, Y. Iqbal, W. Hanke, A. P. Schnyder, M. M. Denner, M. H. Fischer, T. Neupert, and R. Thomale, arXiv preprint arXiv:2104.05671 (2021).